WestVirginiaUniversity
THE RESEARCH REPOSITORY @ WVU

Faculty Scholarship

2016

Sensitive 21 cm observatios of neutral hydrogen in the local group near M31

Spencer A. Wolfe

Felix J. Lockman

D. J. Pisano

Follow this and additional works at: https://researchrepository.wvu.edu/faculty_publications

SENSITIVE 21 cm OBSERVATIONS OF NEUTRAL HYDROGEN IN THE LOCAL GROUP NEAR M31

Spencer A. Wolfe[1], Felix J. Lockman[2,3], and D. J. Pisano[1]

[1] Dept. of Physics & Astronomy, West Virginia University, Morgantown, WV 26506, USA; swolfe4@mix.wvu.edu, DJPisano@mail.wvu.edu

[2] National Radio Astronomy Observatory, Green Bank, WV 24944, USA; jlockman@nrao.edu

ABSTRACT

Very sensitive 21 cm H I measurements have been made at several locations around the Local Group galaxy M31 using the Green Bank Telescope at an angular resolution of $9'.1$, with a 5σ detection level of $N_{H\,I} = 3.9 \times 10^{17}\,\mathrm{cm}^{-2}$ for a $30\,\mathrm{km\,s}^{-1}$ line. Most of the H I in a 12 square-degree area almost equidistant between M31 and M33 is contained in nine discrete clouds that have a typical size of a few kpc and a H I mass of $10^5 M_\odot$. Their velocities in the Local Group Standard of Rest lie between -100 and $+40\,\mathrm{km\,s}^{-1}$, comparable to the systemic velocities of M31 and M33. The clouds appear to be isolated kinematically and spatially from each other. The total H I mass of all nine clouds is $1.4 \times 10^6 M_\odot$ for an adopted distance of 800 kpc, with perhaps another $0.2 \times 10^6 M_\odot$ in smaller clouds or more diffuse emission. The H I mass of each cloud is typically three orders of magnitude less than the dynamical (virial) mass needed to bind the cloud gravitationally. Although they have the size and H I mass of dwarf galaxies, the clouds are unlikely to be part of the satellite system of the Local Group, as they lack stars. To the north of M31, sensitive H I measurements on a coarse grid find emission that may be associated with an extension of the M31 high-velocity cloud (HVC) population to projected distances of ~100 kpc. An extension of the M31 HVC population at a similar distance to the southeast, toward M33, is not observed.

Key words: galaxies: halos – galaxies: ISM – intergalactic medium – Local Group

1. INTRODUCTION

The two largest galaxies in the Local Group, M31 and the Milky Way, have a substantial amount of gas residing in a circumgalactic medium (CGM, also called a gaseous halo), outside of their disks. Their CGM is dominated by ionized gas, but also contains neutral high-velocity clouds (HVCs) observed in the 21 cm line (Wakker 2001; Sembach et al. 2003; Thilker et al. 2004; Westmeier et al. 2008; Putman et al. 2009; Shull et al. 2009; Lehner et al. 2012, 2015). Gas likely associated with M31 is seen in absorption against background AGNs to projected distances of at least 300 kpc (Lehner et al. 2015). The Milky Way may have a similar CGM less easily separated from disk gas because of projection effects, but manifested in the stripping of gas from dwarf spheroidals at distances to 300 kpc (Grcevich & Putman 2009; Gatto et al. 2013; Spekkens et al. 2014). If the CGM of M31 does extend this far, it encompasses the smaller spiral M33, which itself has a modest population of neutral HVCs (Grossi et al. 2008; Putman et al. 2009). The CGM of the Milky Way contains the Magellanic Stream (MS), which extends at least 200° across the sky in H I emission and whose mass is probably dominated by ionized gas (Nidever et al. 2010; Fox et al. 2014).

There are also neutral atomic hydrogen (H I) clouds in the Local Group whose connection with individual galaxies is not understood. Compact high-velocity clouds (CHVCs) and ultra-compact high-velocity clouds (UCHVCs) are of small angular size and are relatively isolated, and are candidates for low-mass galaxies that may lack star formation entirely (de Heij et al. 2002; Adams et al. 2013). For a variety of reasons, CHVCs are now thought to reside in the Milky Way CGM (e.g., Sternberg et al. 2002), but the location and nature of the recently discovered UCHVCs is less clear.

In their study of 21 cm emission from H I in the Local Group, Braun & Thilker (2004, hereafter BT04) discovered extended regions of H I around the galaxy M31 that formed a partial bridge to the galaxy M33. This emission was detected at the extremely low levels of $N_{H\,I} \sim 10^{17}\,\mathrm{cm}^{-2}$, about two orders of magnitude below the typical column density detectable in extragalactic 21 cm observations (Heald et al. 2011). The BT04 observations were made with a rather coarse angular resolution of 49′ and the origin of the neutral gas was uncertain, but the diffuse H I appeared to connect the systemic heliocentric velocities of M31 and M33 (Lewis et al. 2013). BT04 proposed that the H I arose from condensation in a dark matter-dominated filament connecting the two galaxies. Another suggestion was that it resulted from a tidal encounter between the galaxies (Bekki 2008). Subsequent observations of part of the region using the Green Bank Telescope (GBT) at 9′ angular resolution confirmed the reality of the emission, though those data lacked the sensitivity to reveal any detailed structure (Lockman et al. 2012). As the existence and properties of CGM and intra-group gas is critical to our understanding of the formation and evolution of galaxies (e.g., Davé et al. 2001; Fukugita & Peebles 2006; Chen et al. 2010; Putman et al. 2012; Cen 2013; Lehner et al. 2015), we have undertaken a major survey of the area around and between M31 and M33 using the GBT, which provides both the sensitivity needed to detect this extremely faint emission, and the angular resolution to discern some of its structure.

In a previous paper (Wolfe et al. 2013, hereafter Paper I) we presented the results of the first part of the study, which showed that a significant fraction of the H I detected in a 12 square-degree field southeast of M31 in the direction of M33 arose in discrete structures, which, assuming they are 800 kpc distant, have the size of dwarf galaxies but no detectable stellar component. Subsequently, Martin et al. (2013) suggested that there may be a stellar overdensity in the direction of one of the clouds, but the association between the gas and stars is not
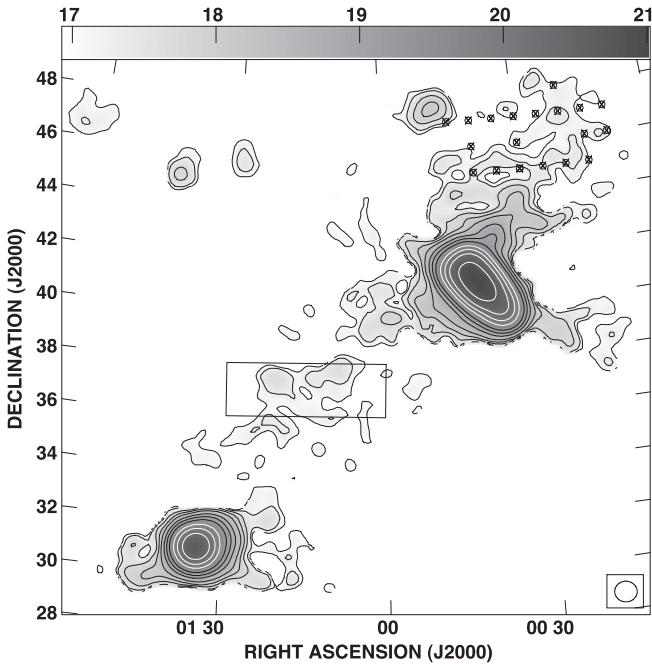

Figure 1. Locations of the current observations marked on a map of the total $N_{H\,I}$ from the BT04 survey. The galaxies M33 and M31 lie at the lower left and upper right, respectively. Contours are for $\log(N_{H\,I}) =$ 17.0, 17.3, 17.7, 18.0, 18.3, 18.7, 19.0, 19.3, 19.7, 20.0, 20.3, and 20.7 (cm^{-2}). Our "M31–M33" field, outlined with a box, lies between the two galaxies and was covered with complete sampling. North of M31, we made a series of pointed observations at locations marked with boxed crosses. The GBT angular resolution is 9′, but the boxed crosses are 15′ in size to make them easier to see. The boxed circle in the lower right shows the resolution of BT04.

established at this time. The clouds have velocities similar to the systemic velocities of M31 and M33 and are thus probably not part of the HVC system of either galaxy. Here we report on additional observations that reveal more clearly the structure and content of the H I clouds, as well as new observations of selected directions to the north of M31. The distances to M31 and M33 are ~750 and ~850 kpc, respectively (e.g., Bono et al. 2010; Riess et al. 2012), so we assume that the material located between them lies at a distance of 800 kpc.

2. OBSERVATIONS

All data used here were obtained with the 100 m GBT (Prestage et al. 2009) with the dual-polarization L-band receiver that has a total system temperature of $\lesssim 18$ K at elevations $>20°$. At the frequency of the 21 cm line, the telescope has a half-power beam-width of 9′.1. Spectra were measured using the GBT Spectrometer, which provides a total velocity coverage >1000 km s^{-1} in the 21 cm line at a channel spacing of 0.32 km s^{-1}. Spectra were calibrated using observations of 3C48 and the antenna response analysis from Boothroyd et al. (2011). Velocities were measured with respect to the Local Standard of Rest (LSR), but in this part of the sky V_{LSR} differs from heliocentric velocities by only a few km s^{-1}.

Figure 1 shows the observed areas on the BT04 H I map of the region. Data reduction was done with special procedures written in GBTIDL (Marganian et al. 2006), the stray radiation correction and calibration followed Boothroyd et al. (2011), and special procedures were written to remove instrumental baselines from spectra in the data cube.

2.1. The M31–M33 Field

As described in Paper I, we used the GBT to map a $6° \times 2°$ field in R.A. and decl. centered at J2000 $= 01^h16^m + 37°00′$. The observations were made while moving the telescope in R. A. at a fixed decl., binning the data in 3-s samples every 1′.6 in R.A. At the end of the $6°$ strip the telescope was stepped in decl. by 3′.6 and the scanning direction was reversed. This procedure covered the area with Nyquist sampling in decl., and finer sampling in the moving coordinate to prevent beam broadening (Mangum et al. 2007). Regions at the eastern edge of each row—areas identified as having no emission by BT04 and confirmed from our observations—were used as reference positions. Spectra from the easternmost 16′ of each strip were averaged and supplied the reference spectrum for the rest of the spectra in the strip. As the reference spectrum had an integration time of 30 s, this greatly reduced the noise in the difference spectrum. The field was observed over and over again until the desired noise level was reached. In total, the M31–M33 field was observed for about 400 hr with an average time per GBT beam of 46 minutes. Our observing procedure could cancel some emission, but only if it had a nearly constant amplitude and V_{LSR} over scales of many degrees. We see no evidence of this in the data. There are three positions in our map where Lockman et al. (2012) made frequency-switched detections of H I emission associated with the clouds. Those data are in reasonable agreement with our current measurements. At another position where only a small upper limit was reported, we likewise see no emission. This indicates that our position-switched technique has not cancelled significant amounts of H I. In addition, the current data are consistent with the sensitive GBT spectrum reported in BT04, but note that the decl. reported in BT04 has a typographical error: the correct position of the GBT spectrum is J2000 $= 01^h20^m29″ + 37°22′33″$.

Spectra were corrected for atmospheric attenuation and a second-order polynomial was fit to emission-free channels to provide statistics for a quick check on data quality. In general, instrumental baselines were excellent and modeled well by a second or third-order polynomial. A small fraction of the spectra (4%) was rejected for having poor instrumental baselines caused mainly by radio frequency interference or temporary instrumental effects. The spectra were smoothed to an effective velocity resolution of 5.15 km s^{-1} and gridded into a cube using AIPS[4] with a pixel spacing of 1′.75 using a spherical Bessel interpolation function following Mangum et al. (2007). A third-order baseline was removed from each spectrum in the cube. The procedure of subtracting a nearby reference position should effectively remove stray radiation (Boothroyd et al. 2011), hence no further corrections were applied. The noise in the final cube varies slightly with position, with a typical value, in brightness temperature, of $\sigma_T = 3.45$ mK in a 5.15 km s^{-1} channel. This gives a 5σ limit on $N_{H\,I}$ of 3.9×10^{17} for a 30 km s^{-1} full width at half maximum (FWHM) line. The equivalent H I mass limit is $\sim 10^4\, M_\odot$, assuming a distance of 800 kpc. We note that previous surveys around galaxy groups typically have mass limits $\gtrsim 10^5\, M_\odot$ (Auld et al. 2006) or $10^6\, M_\odot$ (e.g., Zwaan 2001; Pisano et al. 2007; Chynoweth et al. 2008).

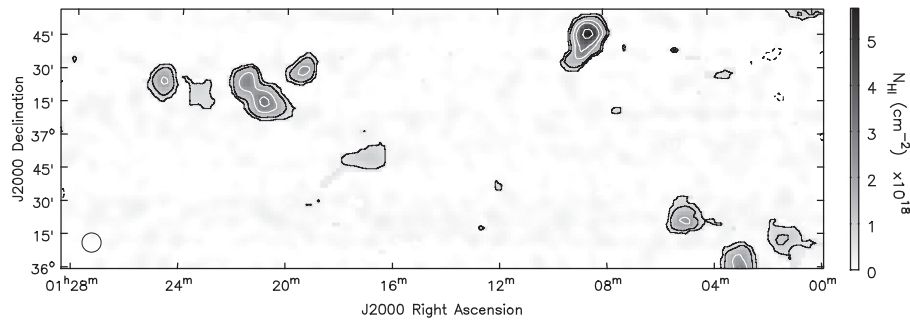
[4] Developed by the National Radio Astronomy Observatory: http://www.aips.nrao.edu/index.shtml.

Figure 2. Integrated H I column density map of the M31–M33 clouds over $-359 \leqslant V_{\mathrm{LSR}} \leqslant -187$ km s^{-1}. The contours are at -1, 1, 2, 4, 6, and 10 times increments of 5×10^{17} cm^{-2}. The circle in the lower left shows the angular resolution of the GBT.

2.2. M31 North Observations

Observations were also made at 18 positions north of M31 to investigate the nature of the very faint 21 cm emission detected by BT04 in this area. The observed positions are shown in Figure 1. Here, because reference positions were not readily available, the data were taken by frequency switching between the 21 cm rest frequency and a band 4 MHz (844 km s^{-1}) away within the 12.5 MHz band of the GBT Spectrometer. Data were calibrated and corrected for stray radiation as described by Boothroyd et al. (2011), and a third or fourth order polynomial was fit to emission-free velocities. The data were then smoothed from 0.3 km s^{-1} velocity resolution to 1.3 km s^{-1}. The typical on-source integration time for each pointing is 76 minutes and the median noise in a 1.3 km s^{-1} channel is 3.7 mK. This gives a 5σ limit on $N_{\mathrm{H\,I}}$ of 1.6×10^{17} cm^{-2} for a spectral line with a FWHM of 30 km s^{-1}.

3. NEUTRAL HYDROGEN BETWEEN M31 AND M33

An integrated intensity map of the spectra summed over $-359 \leqslant V_{\mathrm{LSR}} \leqslant -187$ km s^{-1} and converted to column density, $N_{\mathrm{H\,I}}$, is presented in Figure 2. This range encompasses all detected H I emission not associated with the Milky Way. Emission from the disks of M31 and M33 overlaps that from the Milky Way at some $V_{\mathrm{LSR}} \geqslant -150$ km s^{-1}, but these velocities are not in the range studied here. $N_{\mathrm{H\,I}}$ is calculated under the assumption that the emission is optically thin, an excellent assumption for lines with $T_b < 100$ mK. The rms noise in column density is 1.9×10^{17} cm^{-2} (1σ); contours are drawn in multiples of 5×10^{17} cm^{-2}. The H I emission in this field is dominated by discrete clouds, some of which are resolved by the GBT $9.'1$ beam. Six of these clouds were detected at full angular resolution in Paper I, the other three appear in the more sensitive data presented here. Spectra toward the peak $N_{\mathrm{H\,I}}$ of each cloud are shown in Figure 3.

A Gaussian function was fit to the 21 cm spectrum of each cloud at the location of its peak $N_{\mathrm{H\,I}}$, and the components, along with the location of the peak, are given in Table 1. Errors are 1σ from the Gaussian fit. Clouds are numbered for convenience; the identification is usually not the same as in Paper I.

Table 2 gives derived properties of the clouds. The velocity with respect to the Local Group (V_{LGSR}) was determined using the calculator given in NED.[5] The quantity *Diam* is the

maximum cloud extent measured down to the 3σ noise level, while $\langle Diam \rangle$ is the diameter of a circle with an area equal to that of the cloud. The difference between these quantities is a measure of the elongation of a cloud. The "average FWHM" of the 21 cm line averaged over the entire cloud is given in Col. 5. Cloud 8 was not completely mapped so some of its quantities are limits. There is an additional emission feature at the very northwest edge of the field, J2000 = 01^{h}00^{m}24^s + 37°53′ with $T_L \approx 10$ mK at $V_{\mathrm{LSR}} = -264$ km s^{-1} and a peak $N_{\mathrm{H\,I}} \lesssim 10^{18}$ cm^{-2}, but we cannot characterize it further.

The H I mass in Col. 7 was calculated by integrating over velocities relevant to each cloud, then summing over an area around the cloud. The mass assumes that the emission is optically thin. Errors on the mass are derived from the noise in emission-free channels over the area of each cloud.

A two-dimensional Gaussian was fit to each cloud yielding a major and minor axis size. For this, the two parts of Cloud 3 were treated separately. Major and minor axis radii from the Gaussian fitting were then deconvolved to produce an estimate of the true angular size given the $9.'1$ beam of the GBT, which is approximately Gaussian: $r_{\mathrm{true}} = (r_{\mathrm{obs}}^2 - 4.'55^2)^{1/2}$. The minor axis of Clouds 1, 3b, and 4 were unresolved within the errors, and for these we assume an intrinsic radius of $1'$, equivalent to 233 pc at the assumed 800 kpc distance of the clouds. Quantities derived from this adopted radius are consequently uncertain, and are marked with a colon (:) in Table 2. The square root of the product of the deconvolved major and minor axis radii is given in Col. 6 of Table 2 and called $r_{1/2}$. This is the average radius within which half the H I mass is contained as estimated from the deconvolved Gaussian fit.

Using this radius we calculate a dynamical (or virial) mass– the total mass (from whatever source) needed to bind a cloud of radius $r_{1/2}$ that has a given velocity dispersion. We note that the definition of the *dynamical* or *virial* or *total* mass derived from the size and velocity structure of an object differs considerably from author to author, and an exact determination requires information that we do not possess, such as the density structure within a cloud. For simplicity, and to allow comparisons with other measurements (see Section 6) we adopt the following (Binney & Tremaine 2008):

$$M_{\mathrm{dyn}} \equiv \frac{2\, r_{1/2}\, \sigma_{\mathrm{v}}^2}{G}, \tag{1}$$

where G is the gravitational constant and σ_{v} is the three-dimensional velocity dispersion of the cloud. As σ_{v} is not a measurable quantity, we use the FWHM from the measured

---

[5] The NASA/IPAC Extragalactic Database is operated by the Jet Propulsion Laboratory, California Institute of Technology, under contract with the National Aeronautics and Space Administration.
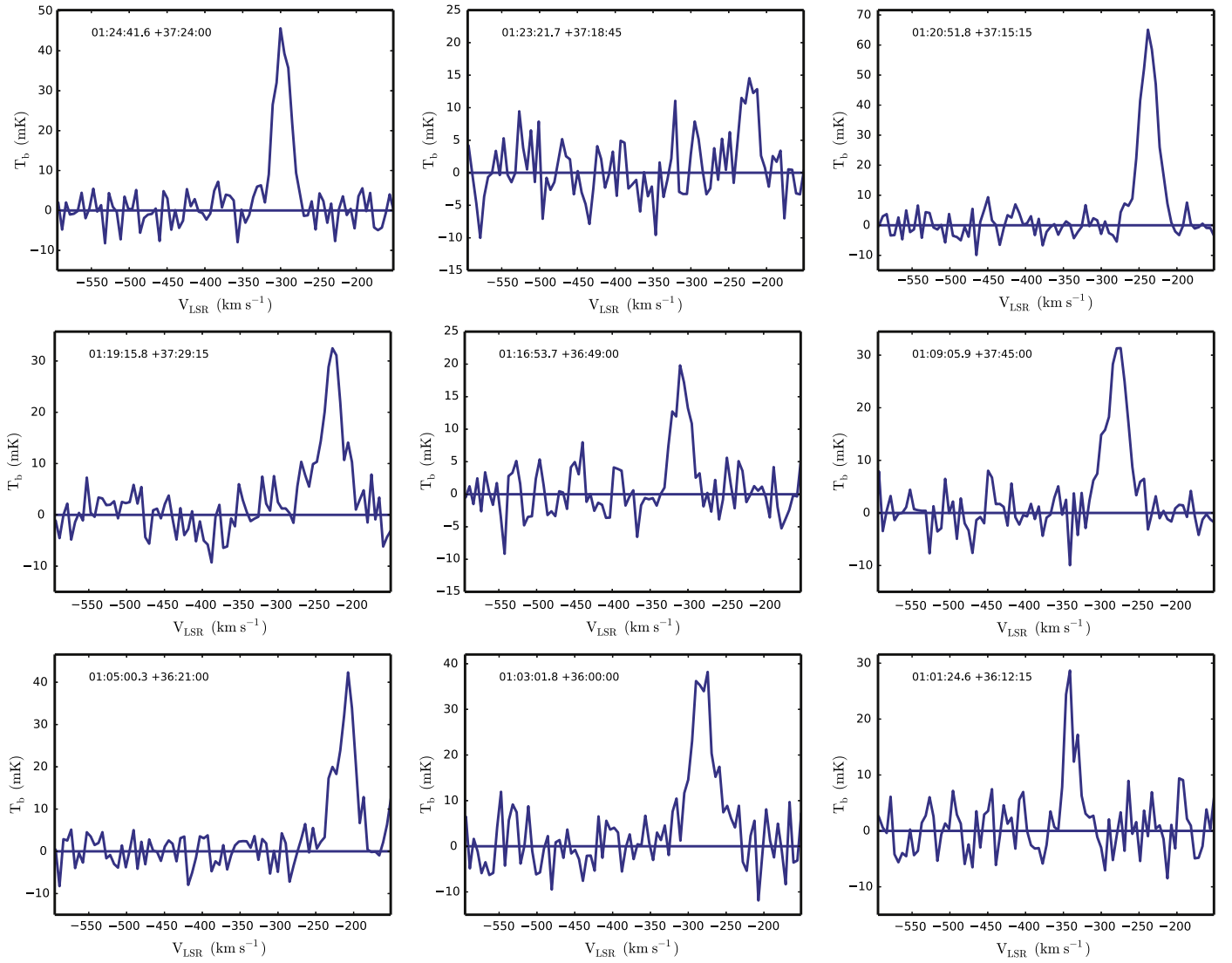
Figure 3. Spectra taken at the peak $N_{\mathrm{H\,I}}$ of the nine clouds detected in the M31–M33 field. The vertical axis is 21 cm brightness temperature and the horizontal axis is V_{LSR}.

Table 1
Clouds Detected Between M31 and M33

Cloud	J2000 (hh:mm:ss dd:mm:ss)	T_{L} (mK)	FWHM (km s^{-1})	V_{LSR} (km s^{-1})	$N_{\mathrm{H\,I}}$ (10^{18} cm^{-2})
(1)	(2)	(3)	(4)	(5)	(6)
1	01:24:41.6 +37:24:00	44.0 ± 2.4	25.5 ± 1.6	−297.8 ± 0.7	2.2 ± 0.1
2	01:23:21.7 +37:18:45	10.9 ± 2.2	39.3 ± 9.3	−223.0 ± 4.0	0.8 ± 0.1
3	01:20:51.8 +37:15:15	63.2 ± 1.8	27.2 ± 0.9	−237.3 ± 0.4	3.3 ± 0.1
4	01:19:15.8 +37:29:15	28.5 ± 2.1	38.1 ± 3.3	−228.2 ± 1.4	2.2 ± 0.1
5	01:16:53.7 +36:49:00	18.3 ± 1.7	26.2 ± 3.0	−308.7 ± 1.2	0.9 ± 0.1
6	01:08:29.6 +37:45:00	81.3 ± 3.6	32.0 ± 1.9	−278.6 ± 0.6	5.0 ± 0.1
7	01:05:00.3 +36:21:00	34.7 ± 3.0	31.4 ± 3.5	−210.2 ± 1.2	2.1 ± 0.2
8	01:03:01.8 +36:00:00	35.0 ± 2.6	36.8 ± 3.4	−281.4 ± 1.3	2.5 ± 0.2
9	01:01:24.6 +36:12:15	25.4 ± 3.2	19.2 ± 2.9	−341.0 ± 1.2	0.9 ± 0.1

average spectrum, and assume isotropy to calculate

$$\left(\frac{M_{\mathrm{dyn}}}{M_\odot}\right) \equiv 2.5 \times 10^5 \left(\frac{r_{1/2}}{\mathrm{kpc}}\right)\left(\frac{\mathrm{FWHM}}{\mathrm{km\,s^{-1}}}\right)^2, \qquad (2)$$

where $r_{1/2}$ is in kpc, FWHM in km s^{-1} and M_{dyn} is in solar masses. Dynamical masses are given in Col. 8. In all cases they

exceed the observed H I mass by a factor of $\sim 10^3$. Col. 9 gives ρ, the projected distance from M31 assuming that the clouds are at a distance of 800 kpc. The clouds lie $\gtrsim$90 kpc away from M31's center, farther than the distances of the known HVCs around M31, all of which have $\rho < 50$ kpc (Westmeier et al. 2008).

4

Table 2
Derived Cloud Properties[a]

Cloud	V_{LGSR} (km s^{-1})	Diam[b] (kpc)	$\langle$Diam$\rangle$[c] (kpc)	$\langle$FWHM$\rangle$[d] (km s^{-1})	$r_{1/2}$[e] (kpc)	$M_{H\,I}$ ($10^4 M_\odot$)	M_{dyn}[f] ($10^8 M_\odot$)	ρ[g] (kpc)
(1)	(2)	(3)	(4)	(5)	(6)	(7)	(8)	(9)
1	−61	4.4	3.2	22.2 ± 0.6	0.38:	12.7 ± 0 .2	0.5:	126
2	+14	4.4	2.8	28.0 ± 3.5	0.75	4.5 ± 0.2	1.5	123
3	+1	7.2	5.3	27.6 ± 0.8		33.0 ± 0.3	⋯	118
3a	⋯	⋯	⋯	28.0 ± 1.0	0.82	22.7 ± 0.2	1.6	⋯
3b	⋯	⋯	⋯	27.1 ± 1.3	0.34:	10.2 ± 0.2	0.6:	⋯
4	+12	3.7	3.1	26.5 ± 1.5	0.41:	8.6 ± 0.2	0.7:	112
5	−69	7.0	3.8	21.8 ± 2.5	1.13	7.8 ± 0.2	1.3	109
6	−32	7.2	4.6	33.6 ± 1.3	0.78	39.2 ± 0.3	2.2	87
7	+36	4.9	3.9	27.4 ± 2.1	0.71	12.6 ± 0.4	1.3	92
8	−35	>3.5	>3.2	29.6 ± 2.1	⋯	>11.6	⋯	91
9	−94	3.5	3.2	20.5 ± 2.3	0.96	8.7 ± 0.2	1.0	88

Notes.
[a] For an assumed distance of 800 kpc.
[b] Maximum cloud extent.
[c] Diameter of a circle with an area equal to that of the cloud.
[d] Column density weighted average FWHM over the entire cloud.
[e] Square root of the product of the major and minor axis radii.
[f] From Equation (2).
[g] Projected distance from M31.

3.1. The Velocity Range

In the field of Figure 2, we find no H I emission at velocities more negative than that associated with cloud 9, i.e., nothing at $V_{LSR} \lesssim −370$ km s^{-1} and no emission at the more positive velocities between $−190 \lesssim V_{LSR} \lesssim −160$ km s^{-1}. At a still more positive V_{LSR}, there is a band of H I extending from the south center of the field to the northwest that is quite bright by our standards ($T_b > 0.6$ K) at $−150 \lesssim V_{LSR} \lesssim −100$ km s^{-1}. This appears to connect smoothly to Milky Way emission at a more positive velocity and we will not consider it further here.

Lehner et al. (2015) argue that the CGM of M31 should be defined as having $−300 \lesssim V_{LSR} \lesssim −150$ km s^{-1}, that velocities more negative than this may arise in the MS and velocities more positive in the halo of the Milky Way. Our Cloud 9 has a peak $N_{H\,I}$ at $V_{LSR} = −341$ km s^{-1}, but is in no way unusual in its size, mass, line width, or projected distance from M31, so we assume that it is part of the cloud population. Westmeier et al. (2008) have detected 21 cm emission that they attribute to M31 HVCs only ~2° to the northwest of the Figure 2 field at velocities as negative as $V_{LSR} \approx −500$ km s^{-1}. We would have easily detected similar emission in the Figure 2 field. Apparently the M31 HVC population does not extend over this area. This will be discussed further in Section 6.

3.2. The Total Neutral Hydrogen Mass

Figure 2 shows some evidence for H I emission outside of the clouds listed in Table 1, but this is relatively small and usually concentrated in discrete regions. Assuming that all the H I we detect is at a distance of 800 kpc, the sum of the H I mass of all nine clouds is $1.4 \times 10^6 M_\odot$, while integration over the entire field yields $1.6 \times 10^6 M_\odot$. Thus virtually all of the neutral gas we measure is contained in the nine clouds, with about half in just the two largest clouds, numbers 3 and 6.

To compare our data with those of BT04, we match the angular resolution of that survey by convolving the integrated spectra shown in Figure 2 to an angular resolution of 49′ using the WSRT beam from Popping & Braun (2008). Results are

shown in Figure 4. While the maps have many similarities there are significant differences. The most striking is near J2000 = 01^{h}13^{m}30^s, +37°24′, where the BT04 data show emission that does not appear in the GBT data. The BT04 survey also contains emission at the south-central part of our field, some of which may arise from a cloud just off our map at 01^{h}10^m, +35°30′ convolved with the much larger BT04 beam. In some areas we find good agreement between the two surveys–the northwest and northeast corners, for example–but overall BT04 reports an H I mass $2.5 \times 10^6 M_\odot$ for the area, while we find only 63% of this amount.

We believe that the cause of this discrepancy lies mostly, though not entirely, in the choice of velocity range of integration for the BT04 survey. No emission is detected with the GBT at velocities more negative than $−370$ km s^{-1}. If the GBT data are integrated over all velocities $\leqslant −150$ km s^{-1}, the total mass remains $1.6 \times 10^6 M_\odot$, but if the upper limit is taken to be $−140$ km s^{-1}, only 10 km s^{-1} more positive, the total H I mass doubles. We discuss the above reasons for not including emission at $V_{LSR} \geqslant −150$ km s^{-1} in the census of Local Group gas, as it likely arises in the Milky Way (Lehner et al. (2015) conclude this as well). It is plausible that some of this emission is present in the BT04 map, especially as those spectra had a rather coarse velocity resolution of 17 km s^{-1}. This explanation does not account for the discrepancy with the BT04 feature at 01^{h}13^{m}30^s + 37°24′. The GBT spectrum in this direction is entirely consistent with noise at $V_{LSR} \leqslant −145$ km s^{-1}.

In Paper I we reported that there was $\approx 1 \times 10^6 M_\odot$ of H I in the GBT data that was not associated with discrete clouds. We now believe that this conclusion is incorrect and resulted from a very small systematic baseline error with an amplitude of only a few mK in the preliminary GBT data. In the current data there can be no more than $0.2 \times 10^6 M_\odot$ of H I outside the nine clouds. We do not believe that our data reduction procedure is artificially suppressing real emission; instrumental baseline fitting removes only low-order polynomials preserving lines of normal velocity width, and the position-switching observing technique preserves structure on angular scales $\lesssim 5°$. If there
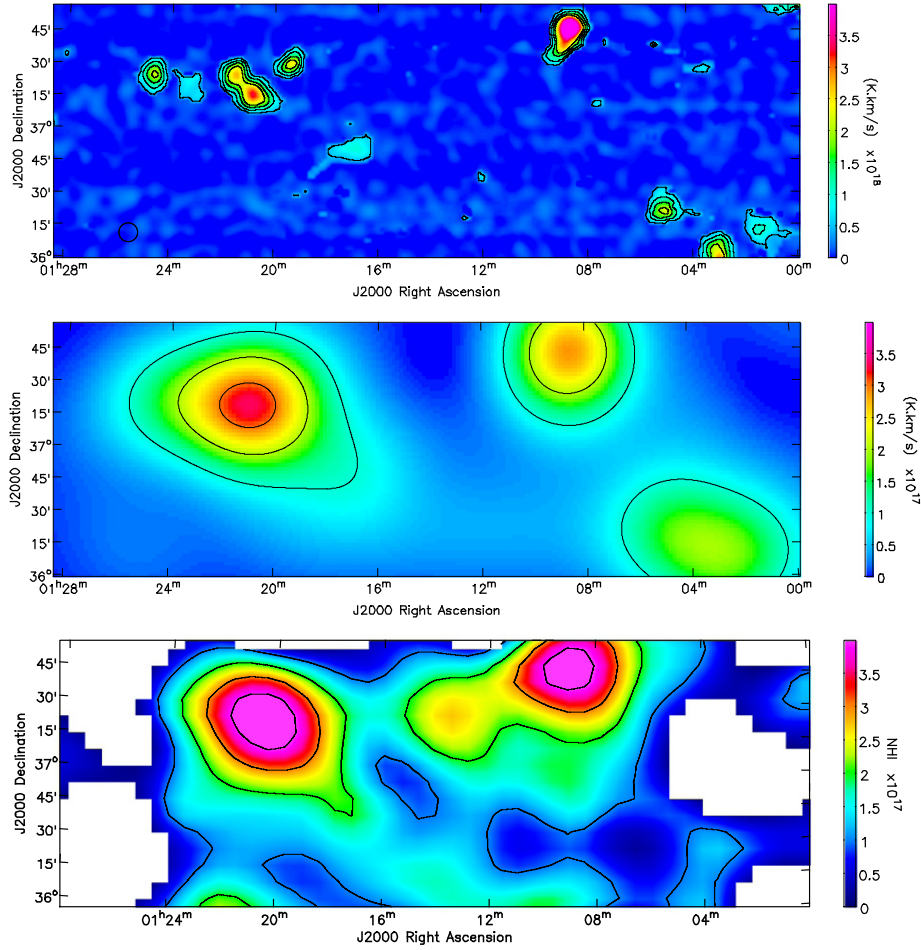
Figure 4. Top panel: integral column density of the M31–M33 field at full GBT angular resolution; contours are every 5×10^{17} cm^{-2} beginning at 5×10^{17} cm^{-2} and the color scale runs from zero to 4×10^{18} cm^{-2}. Middle panel: GBT data smoothed to the $49'$ angular resolution of the BT04 measurements using the WSRT beam from Popping & Braun (2008). For this and the lower panel, the color scale runs from zero to 4×10^{17} cm^{-2}, and the contours are every 10^{17} cm^{-2} beginning at 10^{17} cm^{-2}. Lower panel: BT04 integral column density map at $49'$ resolution. Regions without detectable H I are blanked. While many of the general features of our GBT data agree with those from BT04, the BT04 map contains regions of emission not found in the GBT data.
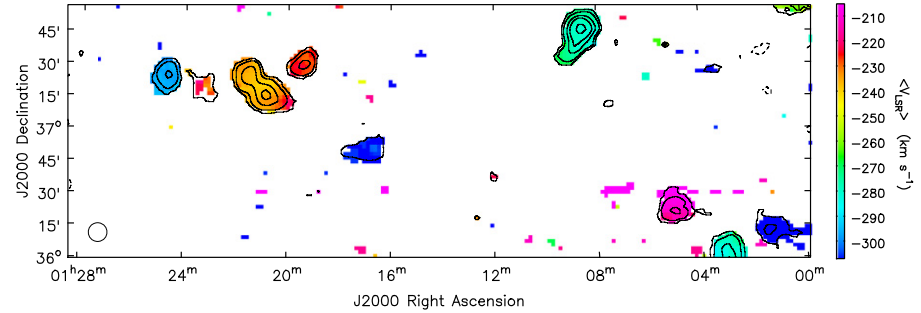

Figure 5. Average V_{LSR} over the field, calculated for channels between $-359 \leqslant V_{LSR} \leqslant -187$ km s^{-1} that have $T_b > 4\sigma = 0.015$ K. Although velocities can vary significantly from cloud to cloud, the mean velocity within a cloud is relatively constant. The circle in the lower left shows the angular resolution of the GBT. It is apparent that the clouds are separated not only spatially but kinematically.

was emission in the reference regions beyond the edge of the map, we would see it as negative features in the map. As no such features exist, we have confidence in our estimates of $M_{H I}$.

3.3. Velocity and Line Width

The average velocity of the H I emission is shown pixel-by-pixel in Figure 5. Contours are the same as in Figure 2. Here, to give an indication of the overall velocity pattern of the clouds

the velocity-weighted values of the brightness temperature were calculated over the entire range of detectable emission: -359 to -187 km s^{-1}, clipping the data at the approximate 4σ noise level of 15 mK. The clouds span a range of velocity between $-341 \leqslant V_{LSR} \leqslant -210$ km s^{-1}. In our data, there are only two clouds that have significant internal velocity structure. These are shown in Figures 6 and 7.

Cloud 3 consists of two components with nearly identical velocities at their peak, but overall there is a 10 km s^{-1} gradient
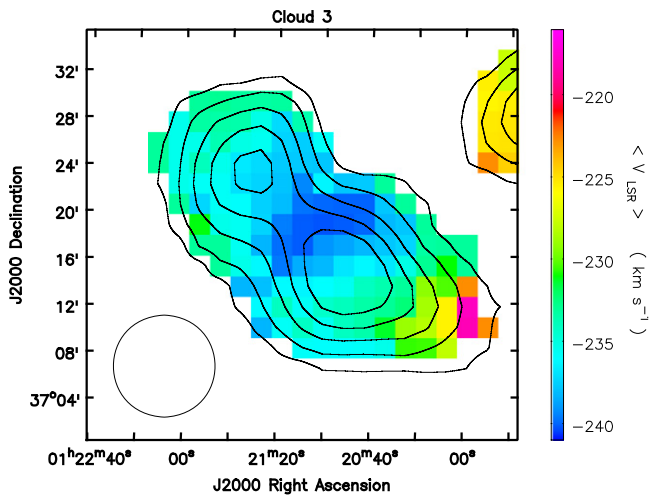
Figure 6. Average V_{LSR} pixel-by-pixel for Cloud 3 together with contours of $N_{H I}$. Averages were calculated only for channels with $T_b > 4\sigma = 15$ mK. Contours are at 1, 2, 3, 4, and 5 times increments of 5×10^{17} cm^{-2}. Unrelated emission from Cloud 4 appears in the upper right. The circle in the lower left shows the angular resolution of the GBT. Both cloud components show a 10 km s^{-1} velocity gradient between their center and edge.
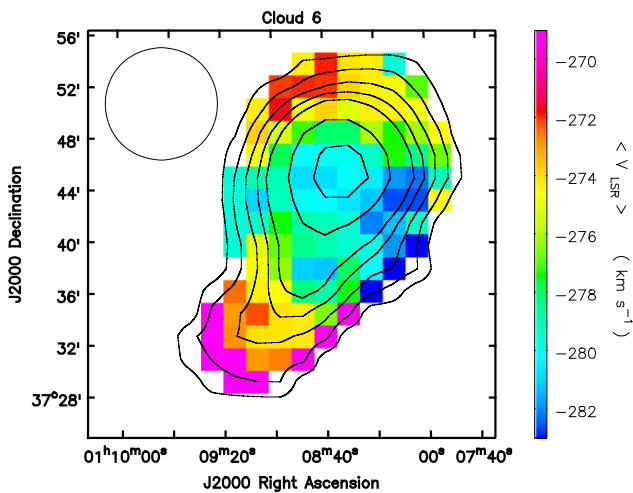

Figure 7. Average V_{LSR} pixel-by-pixel for Cloud 6 together with contours of $N_{H I}$. Averages were calculated only for channels with $T_b > 4\sigma = 15$ mK. Contours are at 1, 2, 3, 4, 5, 7.5, and 10 times increments of 5×10^{17} cm^{-2}. The circle in the upper left shows the angular resolution of the GBT. This cloud shows a 10 km s^{-1} velocity gradient from the center to its edges.

from -240 km s^{-1} between the two cloud components to -233 km s^{-1} at the northern edge and -230 km s^{-1} at the southern edge. Cloud 6 has a head-tail appearance with, once again, velocities most negative at the center and rising by ≈ 10 km s^{-1} at the northern and southern edges.

The mean line width at the peak $N_{H I}$ of the nine clouds is 27.9 ± 4.3 km s^{-1}, essentially identical to the median. The lines are well-fit by single Gaussians. Unlike Galactic HVCs and CHVCS, there is no evidence for two components in any of the lines as would be expected if they have a two-phase temperature structure (Sternberg et al. 2002). The FWHM does not vary much across an individual cloud. The FWHM averaged over the entire cloud (Table 2) and toward the peak $N_{H I}$ (Table 1) are quite similar. The range of line widths is 19.2–32.5 km s^{-1}, much smaller than the range observed in 17

M31 HVCs (at essentially identical angular resolution) of 11–71 km s^{-1} (Westmeier et al. 2008).

Figure 5 re-enforces the impression from Figure 2 that the individual clouds are independent entities, as nearby clouds can have quite different velocities. Clouds 7 and 9, for example, differ by 120 km s^{-1} yet are separated by $< 1°$ on the sky (~ 10 kpc at 800 kpc distance).

4. NEUTRAL HYDROGEN TO THE NORTH OF M31

Results from the measurements to the north of M31 are given in Table 3, and illustrated in Figure 8 as symbols on a map of the BT04 survey. We include only emission with $V_{LSR} \leqslant -150$ km s^{-1}. Line properties were derived from a Gaussian fit, and errors are 1σ. Values of $N_{H I}$ come also from the Gaussian fit; here errors reflect both the noise and an assumed equal contribution from baseline uncertainties. The median 5σ sensitivity to a 30 km s^{-1} FWHM line is 1.6×10^{17} cm^{-2}. Because we have only incomplete sampling, it is not possible to delineate objects and calculate a mass or size. The values of $N_{H I}$ should be understood as random samples of the medium and not peak values, in contrast to the values given in Table 1 for the M31–M33 field.

Our results are rather puzzling in view of the BT04 data. We detect no emission at $\delta = +45°$, at only one position at $\delta = +46°$, and yet have four detections at $\delta = +47°$, two of which lie outside the lowest BT04 contour. The first conclusion must be that the H I is much patchier than would be inferred from BT04, which does not give a good representation of the H I at $V_{LSR} \leqslant -150$ km s^{-1}. In this sense the M31 north measurements complement the conclusion from the M31–M33 field (Figure 4). In the GBT data, bright lines identified with Milky Way emission are regularly found at $V_{LSR} \approx -100$ km s^{-1}. It is possible that the BT04 map includes some of this material, which might account for the discrepancy with the GBT measurements. Our detection of H I outside the BT04 contours at $\delta = +47°$ would imply that we are seeing very small angular-sized features that suffer from beam dilution in the BT04 measurements. This was also a conclusion from Paper I.

The position at 00^h15^m, $+46°00'$ has two 21 cm line components separated by 150 km s^{-1}. Figure 9(a) shows this spectrum as well as the spectrum at 00^h20^m, $+47°00'$ (9(b)). Both illustrate the emission near -100 km s^{-1} that we attribute to a component of the Milky Way.

5. KINEMATICS OF THE EMISSION

Velocities of all GBT detections are shown in Figure 10 as the Local Group Standard of Rest velocity (V_{LGSR}) versus angular distance from M31. We include both the clouds of Figure 2 and the detections to the north of M31. For comparison, the known HVCs around M31 and M33 are indicated with red circles (Grossi et al. 2008; Westmeier et al. 2008; Putman et al. 2009) and the systemic velocities of M31 and M33 with blue rectangles (Karachentsev & Makarov 1996). As discussed in Paper I, the clouds between M31 and M33 lie at velocities similar to the systemic velocity of both galaxies, and at a larger distance from either galaxy than their HVCs. This is true also of the two newly identified clouds between M31 and M33. Most of the emission to the north of M31 appears to be consistent with arising in an extension of the M31

Table 3
Observations North of M31

| J2000 (hh:mm dd:mm)	Galactic $l°, b°$	σ_T (mK)	T_L (mK)	V_{LSR} (km s^{-1})	FWHM (km s^{-1})	$N_{H\,I}$ (10^{17} cm^{-2})	V_{LGSR} (km s^{-1})	ρ (kpc)
(1)	(2)	(3)	(4)	(5)	(6)	(7)	(8)	(9)
00:10 +46:00	...	3.8	...	...	...	...	...	...
00:10 +47:00	115.6, −15.3	4.4	27.5 ± 1.3	−176 ± 1	25.9 ± 1.4	13.8 ± 1.0	106	115
00:15 +46:00	116.3, −16.4	3.5	15.6 ± 1.2	−238 ± 1	16.0 ± 1.4	4.8 ± 0.6	43	96
		3.5	22.4 ± 1.2	−388 ± 1	23.6 ± 1.4	10.2 ± 0.8	−109	...
00:15 +47:00	...	3.3	...	...	...	...	...	...
00:20 +45:00	...	6.4	...	...	...			
00:20 +47:00	117.4, −15.5	3.3	30.4 ± 1.0	−166 ± 1	26.1 ± 1.0	15.4 ± 0.7	112	98
00:20 +48:00	...	3.6	...	...	...	...	...	...
00:25 +45:00	...	3.8	...	...	...	...	...	...
00:25 +47:00	...	3.7	...	...	...	...	...	...
00:30 +45:00	...	4.1	...	...	...	...	...	...
00:30 +46:00	...	4.4	...	...	...	...	...	...
00:30 +47:00	...	4.5	...	...	...	...	...	...
00:35 +45:00	...	4.1	...	...	...	...	...	...
00:35 +47:00	...	3.7	...	...	...	...	...	...
00:40 +45:00	...	3.3	...	...	...	...	...	...
00:40 +46:00	...	3.8	...	...	...	...	...	...
00:40 +47:00	120.9, −15.8	2.9	18.3 ± 0.7	−182 ± 1	25.1 ± 1.1	8.9 ± 0.6	85	81
00:45 +47:00	121.8, −15.9	3.7	18.8 ± 0.8	−183 ± 1	42.5 ± 2.1	15.5 ± 1.0	86	80
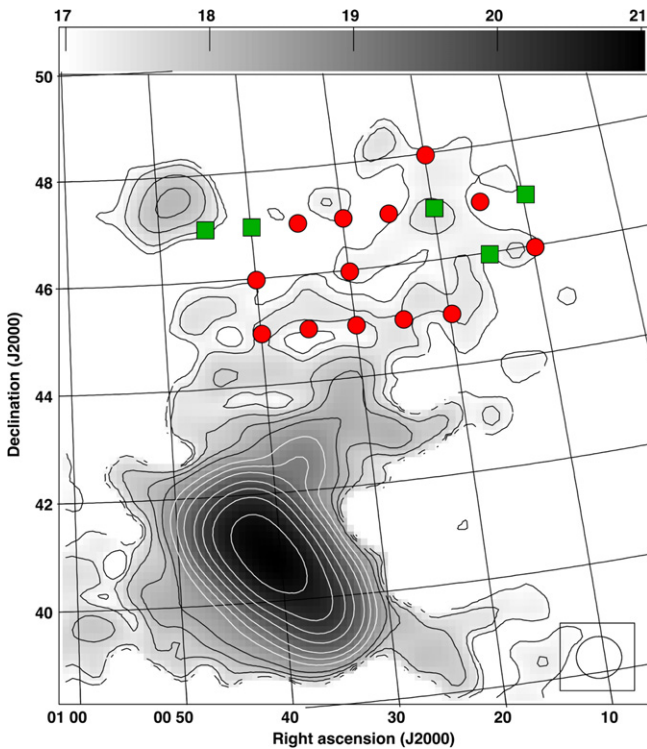
Figure 8. Expanded view of the BT04 survey H I data from Figure 1 to show the locations of the GBT measurements to the northwest of M31. The GBT angular resolution is 9′, but the symbols are 15′ across for easier identification. Green boxes mark positions with detected H I emission at $V_{LSR} \leqslant -150$ km s^{-1}. Red circles show positions without a detection. The circle in the lower right shows the BT04 angular resolution.

Figure 9. (a): spectrum from a deep GBT pointing toward J2000 $= 00^h15^m + 46°00′$. The component at -238 km s^{-1} has a velocity similar to M31's HVCs while the component at -388 km s^{-1} is closer to the systemic velocity of M31. (b): spectrum from a pointing toward J2000 $= 00^h20^m + 47°00′$. The spectral line lies ~50 km s^{-1} from Milky Way emission.

HVC population. It is in the velocity range associated with Lehner et al. (2015) with the CGM of M31.

Koch et al. (2015) report detection of gas possibly associated the M31 Stellar Stream through UV absorption line measurements against background AGNs. Their most secure detection is in lines of Si, C, and O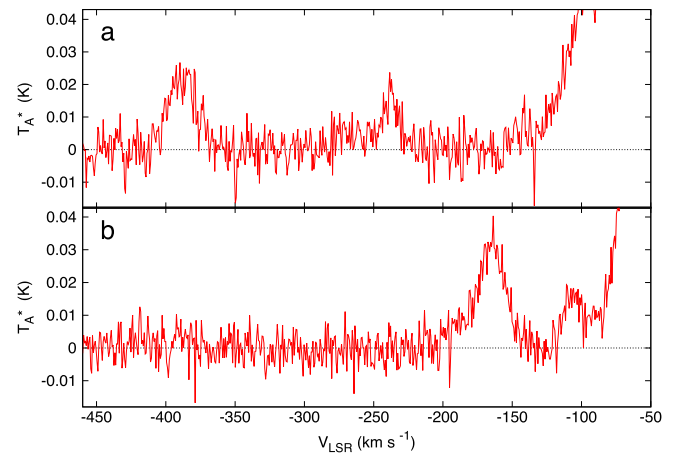 against Q0045+3926 at a location about 2° from M31 in the direction of M33. They find one system at $V_{LSR} = -370$ km s^{-1}, or $V_{LGSR} = -111$ km s^{-1}, which is marked with a pink cross in Figure 10. It lies in the region occupied by M31 HVCs.

The second H I component toward 00^h15^m, $+46°00′$ (Figure 9(a)) at $V_{LSR} = -388$ km s^{-1} ($V_{LGSR} = -109$ km s^{-1}) has a velocity that might be associated with the MS (Lehner et al. 2015) though this direction lies nearly 20° from the axis of the MS as defined by Nidever et al. (2010), and not far from a direction that does not show UV absorption arising in the Stream (Fox et al. 2014). As our measurements are only over a sparse grid in this area, we do not know the size or mass of any cloud associated with this feature. One of the M31 HVCs, the Davies Cloud, has also been suspected of being part of the Stream because its mass would be an order of magnitude larger than the other M31 HVCs if it were at the distance of
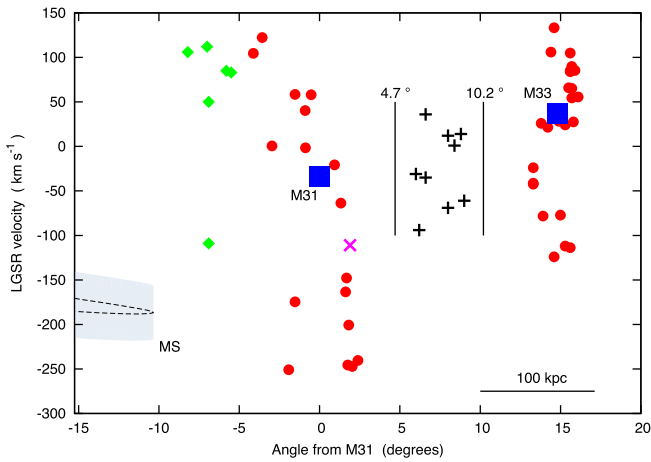
Figure 10. Velocity with respect to the Local Group Standard of Rest (V_{LGSR}) vs. angular distance from M31, where directions toward M33 are taken to be positive. The blue squares are M31 and M33, with the red dots being the high-velocity cloud populations of each galaxy. The black crosses are the clouds from the M31–M33 map with vertical lines marking the map limits. The green diamonds are detections from the GBT pointings north of M31. The pink cross marks the UV absorption line measurements of Koch et al. (2015) toward a background AGN. The MS curve is the estimated position of Stream S0 from Nidever et al. (2010), with a ± 30 km s^{-1} spread to account for the velocity width of the Stream and our approximations. In most cases the Stream lies hundreds of km s^{-1} away from the emission we detect. The rotation of M31 extends from -353 to $+248$ km s^{-1} in V_{LGSR}, and for M33 from -105 to $+158$ km s^{-1} (Braun et al. 2009; Putman et al. 2009).

M31 (Davies 1975; Westmeier et al. 2008). The Davies Cloud does not have extraordinary kinematics and does not occupy an unusual location in Figure 10. At the distance of M31 its H I mass is similar to that of the Milky Way HVC Complex C (Wakker et al. 2007). We see no reason to exclude it from the M31 HVC population.

Because Nidever et al. (2010) have shown that the MS extends into the BT04 area, we have tried to estimate where the MS would lie in Figure 10. Five H I Streams were identified in the BT04 data from (Nidever et al. 2010, Figure 4), labeled S0-S4. We take Stream S0, the one closest to our pointings, to lie along a line of constant RA at 23$^{\mathrm{h}}$45$^{\mathrm{m}}$ and choose a decl. range from $+20$ to $+50$ degrees.

To approximate the LGSR velocities of Steam S0 along this line, we first transform the positions to Magellanic Longitude (L_{MS}, Nidever et al. 2008) and use the extended V_{LSR} versus L_{MS} fiducial curve from Figure 7(b) of Nidever et al. (2010), converting to V_{LGSR}. The resulting angle-velocity for Stream S0 is shown as a dashed curve in Figure 10. To account for the spread in velocity of the Stream, and for our approximations, we overplot a shaded region with bounds of ± 30 km s^{-1} from the curve.

The point of closest approach of S0 to M31 is at an angular distance of $10°.3$ with $V_{\mathrm{LGSR}} = -187$ km s^{-1}. Most of our detections to the northwest of M31 lie at least 225 km s^{-1} from the average velocity of S0 ($V_{\mathrm{LGSR}} \approx -175$ km s^{-1}). The line at 00$^{\mathrm{h}}$15$^{\mathrm{m}} + 46°00'$, $V_{\mathrm{LGSR}} = -109$ km s^{-1} is the only one within $5°$ and 50 km s^{-1} of S0, so excepting this, it seems unlikely that the emission we detect arises in the MS.

6. DISCUSSION: THE ORIGIN OF THE CLOUDS BETWEEN M31 AND M33

In the 12 square-degree area between M31 and M33 observed with the GBT, the faint H I discovered by BT04 is

resolved into at least nine discrete clouds. Here we consider possibilities for the origin of the clouds.

6.1. Products of Galaxy Interactions

Although BT04 surveyed a large area, they found H I at relevant velocities only near a line joining M31 and M33 on the sky (Figure 1), and not widespread in the Local Group. This naturally leads to models where the H I tracks past tidal interactions, as in the M81 group (Yun et al. 1994; Chynoweth et al. 2008). Bekki (2008) modeled the BT04 results as arising from a close encounter between M31 and M33 some 4–8 Gyr ago, and others have also considered an interaction a few Gyr ago as an explanation for features in M33's extended HI distribution and the stellar structures in M31 and M33 (McConnachie et al. 2009; Putman et al. 2009; Lewis et al. 2013). The MS is a good, nearby template of an ongoing galaxy interaction (e.g., Besla et al. 2010; Stanimirovic et al. 2010) but its age is quite uncertain, lying in the range of 0.3–2.0 Gyr (D'Onghia & Fox 2015). The H I mass and average $N_{\mathrm{H\,I}}$ are generally higher than we observe between M31 and M33 (Stanimirović et al. 2008; Nidever et al. 2008, 2010). It is worth noting that as gaseous tidal debris ages it should disperse, causing its $N_{\mathrm{H\,I}}$ to decrease, so the M31–M33 clouds may represent material that is substantially older than is seen in the MS.

A recent study of the evolution of the Local Group has now cast doubt on the possibility that we are observing the relic of a past interaction between M31 and M33, as it indicates that in the last ≈ 12 Gyr, M33 has not been closer to M31 than it is now (Shaya & Tully 2013). The same calculations though, suggest that the dwarf galaxies And II and And XV could have interacted with M31 over the last 0.7 Gyr creating a H I extension toward M33. Since Local Group dwarfs with detectable H I typically have $M_{\mathrm{H\,I}}/L_{\mathrm{V}} \sim 1$ (McConnachie 2012; Spekkens et al. 2014), we can estimate how much H I And II and And XV could have contributed to the M31 CGM. Based on the M_{V} from McConnachie (2012), their total H I mass would be $\sim 10^7 M_\odot$, which is comparable to the total H I mass in the entire filamentary structure between M31 and M33. It seems unlikely, however, that the encounter would leave the nine clouds we detect, each apparently coherent, but spread over a projected distance of 70 kpc with a spread in V_{LGSR} of 130 km s^{-1}. It is clear that more detailed modeling of the Local Group, including its gas, is needed to address these possibilities.

6.2. Dwarf Galaxies

The larger M31–M33 clouds have a H I mass similar to that of some dwarf galaxies, but the clouds are not likely to be associated with stellar systems. Table 4 compares properties of the most massive cloud with dwarf galaxies of a similar H I mass. The dwarf spheroidal And XII is included, as it is one of the faintest of the known M31 satellites, but was detected easily in a recent search for even fainter systems (Martin et al. 2013). To allow for accurate comparisons we calculate dynamical masses from the measured quantities in Table 4, using Equation (2).

Local Group dwarfs with detectable H I typically have a stellar mass similar to their gas mass (Spekkens et al. 2014). For Cloud 6 this would imply $M_{\mathrm{V}} < -8$, and its stars would certainly have been detected already. Martin et al. (2013) report

Table 4
Comparison of an M31–M33 Cloud with Dwarf Galaxies

Object	$r_{1/2}$ (kpc)	FWHM[b] (km s^{-1})	$M_{\rm H\,I}$ ($M_\odot$)	M_* ($M_\odot$)	M_V (mag)	$M_{\rm dyn}$ ($M_\odot$)	References
(1)	(2)	(3)	(4)	(5)	(6)	(7)	(8)
Cloud 6[a]	0.78	34	3.9×10^5	⋯	⋯	2.2×10^8	a
Leo P	0.25	24	9.5×10^5	5.7×10^5	−9.4	3.6×10^7	b, c, d
Leo T	0.17	16	2.8×10^5	1.4×10^5	−8.0	1.1×10^7	e, f, g, h
And XII	0.30	6	⋯	3.1×10^4	−6.4	2.8×10^6	i, j

Notes.
[a] For an assumed distance of 800 kpc.
[b] Of the HI emission except for And XII where it is from the stars.
References. (a) This work; (b) Bernstein-Cooper et al. (2014), (c) Adams et al. (2013), (d) McQuinn et al. (2013), (e) Ryan-Weber et al. (2008), (f) Simon & Geha (2007), (g) Faerman et al. (2013), (h) de Jong et al. (2008), (i) Collins et al. (2010), (j) McConnachie (2012).

a possible stellar feature at the Cloud 6 position, but is considerably fainter than And XII, and if it is actually associated with the Cloud, would imply $M_{\rm H\,I}/M_* > 10$. The dynamical mass of Cloud 6 is also about an order of magnitude higher than that of Leo P, even though Leo P has ∼10 times more baryonic mass. Using the relationship between total mass and M_V from the Local Group data of McConnachie (2012), Cloud 6—indeed most of the clouds detected in HI between M31 and M33—should have a stellar counterpart with $M_V < -13$, whereas the surveys of stars near M31 suggest $M_V > -6$. If Cloud 6 is a galaxy it is one with rather extreme properties. It will be interesting to see if the possible association with a slight stellar overdensity discovered by Martin et al. (2013) reveals a real stellar component of this cloud. The dwarf galaxy Leo P has a small rotational velocity, 15 ± 5 km s^{-1}, comparable to its velocity dispersion (Bernstein-Cooper et al. 2014). As shown in Figure 7, Cloud 6 shows a slight gradient in $V_{\rm LSR}$ from center to edge; at our angular resolution any rotational component is comparable to or smaller than its velocity dispersion.

Another reason why the M31–M33 clouds are not likely to be galaxies is that the stellar satellites of M31 and the Milky Way that lie closer than ≈300 kpc to the parent galaxy are extremely deficient in HI, with mass limits typically well below $10^4 M_\odot$. In some cases $M_{\rm H\,I} \leqslant 100\ M_\odot$ (Grcevich & Putman 2009; Spekkens et al. 2014, R. Beaton, private communication). The two M31 satellite galaxies that lie nearest the M31–M33 field, And II with $V_{\rm LSR} = -187$ km s^{-1}, and And XV with $V_{\rm LSR} = -322$ km s^{-1}, are among those that lack detectable HI emission (Lockman et al. 2012). Apparently M31 and the Milky Way are very efficient at stripping gas from small satellites passing through their CGM (Mayer et al. 2006; Grcevich & Putman 2009; Nickerson et al. 2011; Gatto et al. 2013).

Figure 11 contains the same HI data as Figure 10 but instead of the M31 and M33 HVCs, the location and velocity of dwarf galaxies from McConnachie (2012) are shown. There is no obvious connection between the dwarf galaxies and the HI clouds, as the dwarfs are spread over 400 km s^{-1} while the clouds have an average $V_{\rm LGSR}$ like that of M31 and M33, and a total range of only 130 km s^{-1}.

6.3. HVCs and Dark Matter Sub-halos

Table 5 gives information that allows us to compare the M31–M33 clouds with various populations of HVCs. For the M31–M33 clouds, values are the median from Table 2. For the
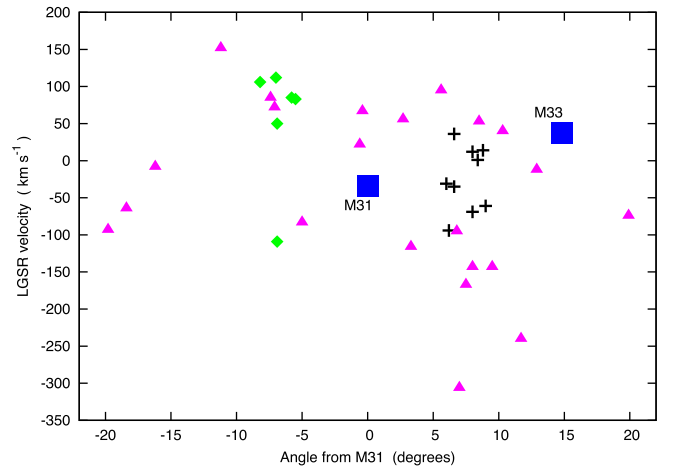

Figure 11. Velocity with respect to the Local Group Standard of Rest ($V_{\rm LGSR}$) vs. angular distance from M31, where directions toward M33 are taken to be positive. The blue squares are M31 and M33, and the black crosses are the clouds from the M31–M33 map. The green diamonds are detections from the GBT pointings north of M31. The pink triangles are dwarf galaxies from the compilation of McConnachie (2012). There is no apparent connection between the dwarf galaxies and the M31–M33 HI clouds.

Table 5
Comparison M31–M33 Clouds with HVCs

Object	$r_{1/2}$ (kpc)	FWHM (km s^{-1})	$M_{\rm H\,I}$ ($M_\odot$)	$M_{\rm dyn}$ ($M_\odot$)	References
(1)	(2)	(3)	(4)	(5)	(6)
M31–M33 Clouds	0.75	27	1.2×10^5	1.4×10^8	a
M31 HVC	0.52	26	4.7×10^5	8.8×10^7	b, c
UCHVC	1.16	23	1.2×10^5	1.5×10^8	d

References. (a) This work; (b) Westmeier et al. (2005), (c) Westmeier et al. (2008), (d) Adams et al. (2013).

M31 HVCs the listed radius is the median found by Westmeier et al. (2005), while the FWHM and $M_{\rm H\,i}$ are the median values from Westmeier et al. (2008). Values for the ultra-compact HVCs (UCHVC) are from Adams et al. (2013), scaled to a distance of 800 kpc.

There is considerable overlap between the physical properties of the M31–M33 clouds and the M31 HVCs, but much less so between their locations and kinematics. Many HVCs are located close to the edge of the M31 disk in intersecting filaments (Westmeier et al. 2005). Although median line widths

are similar, the M31 HVCs have widths as low as half and as high as twice the FWHM of the M31–M33 clouds; 90% have a FWHM in the range 13–67 km s^{-1}, whereas the entire sample of M31–M33 clouds has FWHMs between 19 and 39 km s^{-1}. The HVCs also have a median mass four times larger than the clouds. Indeed, there is no cloud in our sample that has an H I mass as high as the median H I mass of the M31 HVCs. Most importantly, the kinematics of the clouds differ significantly from that of the HVCs near them (Figure 10), and they have a substantially smaller spread in velocity (see also Paper I). With only one exception the detections north of M31 have positions and velocities consistent with being part of the M31 HVC population, while the nine clouds between M31 and M33 do not. The M31 HVCs in the direction of M33 have considerably more negative velocities than the systemic velocity of M31. For M31 $V_{LSGR} = -34$ km s^{-1}, while its HVCs toward M33 have $\langle V_{LGSR} \rangle = -166$ km s^{-1}. In contrast, the M31–M33 clouds have $\langle V_{LGSR} \rangle = -25$ km s^{-1}. The clouds do not appear to be simply an extension of the M31 HVC population. Still, the physical properties displayed in Table 5 suggest that the two populations may be formed by similar processes, and that the UCHVCs, if at a similar distance, have similar properties as well.

Thilker et al. (2004) and Westmeier et al. (2005) considered whether the HVCs of M31 might be the baryonic component of a population of low-mass dark matter halos, an idea with a long history in the study of HVCs (Oort 1966; Blitz et al. 1999; Braun & Burton 1999; de Heij et al. 2002; Nichols et al. 2014). Of particular importance is that some HVCs (and some dwarf galaxies) show a two-component structure in their 21 cm lines, suggesting the presence of gas in equilibrium at two temperatures. This is a diagnostic of pressure, and was used (among other pieces of evidence) to argue that the compact HVCs (CHVCs) must lie at distances $\lesssim 150$ kpc from the Milky Way, and not at distances of ~1 Mpc (Sternberg et al. 2002). The failure to detect CHVC analogs spread throughout other groups of galaxies also implies that they must be located within 90 kpc of individual galaxies (Pisano et al. 2007). This result is consistent with HVC detections around other galaxies such as NGC 891 and NGC 2403 (Oosterloo et al. 2007; Fraternali et al. 2002) and the distance brackets for Milky Way HVCs (e.g., Wakker 2001; Wakker et al. 2007, 2008).

The UCHVCs are discussed in depth in Adams et al. (2013) and Faerman et al. (2013). The dwarf galaxy Leo P was originally classified as a UCHVC on the basis of its 21 cm characteristics before its stellar component was detected and it was discovered to be at a distance of 1.7 Mpc (Giovanelli et al. 2013; McQuinn et al. 2013; Rhode et al. 2013). The H I properties listed in Table 5 for the UCHVCs show that they are similar to the M31 HVCs and the M31–M33 clouds. There is no evidence for a two-phase interstellar medium in the M31 HVCs, the M31–M33 clouds, or in the unidentified UCHVCs, although it is found in other HVCs and the MS (Kalberla & Haud 2006; Stanimirovic et al. 2010). This is important, as it implies that these objects exist in regions of low external pressure (Sternberg et al. 2002). The observations to date, however, have relatively poor linear resolution and might not be able to detect a cool H I phase if present in moderate amounts.

6.4. Gas in Planes of Satellites or a Dark Matter Filament

Lacking an estimate of the distance to the clouds, it is not clear if they are related to the planes of satellite galaxies that are now thought to be fundamental structures in the Local Group (Conn et al. 2012, 2013; Ibata et al. 2013). The M31–M33 field studied here lies in the part of the sky where M31 satellites are aligned in the structure called "Plane 2." It lies to the west of M31 and extends southward toward M33 (Shaya & Tully 2013). The two M31 satellite galaxies nearest to our field on the sky have velocities within the range of the H I clouds (see Figure 3 of Shaya & Tully 2013) and it is an intriguing possibility that the M31–M33 clouds are part of a larger alignment of matter in this part of the Local Group. Although study of these planes is only beginning, if they represent large-scale dark matter structures, then it is very plausible that they would be accompanied by enhancements in gas density.

BT04 suggested that the H I they discovered originated from condensation of hot gas in a dark matter filament connecting M31 and M33. This is now testable, in part, through cosmological simulations that attempt to follow the evolution of systems like the Local Group. Nuza et al. (2014) and Scannapieco et al. (2015) have analyzed the simulation of a group containing two galaxies like M31 and the Milky Way, and while M33 is considerably less massive then the Milky Way, the simulation might still have some application to the M31–M33 region. They find that the hot gaseous halos of the M31 and Milky Way analogs overlap and that they evolve to occupy the same filament, leading to an excess of neutral gas between them that forms around $z \sim 1$ and persists to the present. Clouds like those observed here might then condense in the filament. The current simulations do not have the resolution to detect anything as small as the M31–M33 clouds, and it is not clear that M31 and M33 would have similar overlapping gas halos, but these results are encouraging in that intra-group gas might be a natural feature of systems like the Local Group.

In view of the evidence that M31 has a massive CGM, as discussed in the next section, it will be important to determine if the direction of M33 is enhanced in total material, as would be suggested by this scenario.

6.5. Condensations in the M31 CGM

While the presence of the clouds between M31 and M33 is unexpected, the total mass involved is not large compared to the baryonic mass at that location in the halo of M31 as determined from recent measurements. The observed $N_{H I}$ averaged over our field is only 9×10^{16} cm^{-2}. Lehner et al. (2015) have studied the extended CGM of M31 through measurement of UV absorption lines against background QSOs out to a projected distance >500 kpc, an area that covers not only the M31–M33 clouds, but the galaxy M33 as well. They find that the total gas mass in the M31 CGM may be $>10^{10} M_{\odot}$, with an ionization fraction >90%. The Lehner et al. radial column density profile of Si II evaluated at the projected distance $\rho \approx 100$ kpc of the M31–M33 field predicts $N_{Si II} = 2.1 \times 10^{13}$ cm^{-2}, which implies an average total column density $N_H = 6 \times 10^{17} Z_{\odot}/Z$ cm^{-2}. Thus, if the CGM of M31 has a sub-solar metallicity, even if it is >90% ionized, it would have a neutral component of similar magnitude to the average $N_{H I}$ of the clouds over our field.

The tight kinematic pattern of the M31–M33 clouds suggests that they are not spread along the several hundred kpc path through the M31 halo, so arguments about their origin in the M31 CGM are suggestive at best. The Lehner et al. (2015) measurements, however, allow the possibility that the existence of clouds at $\rho = 100$ kpc from M31 does not require a major enhancement to the mass or density of its CGM, but could result from a restructuring or phase change in material already present, triggered, perhaps, by the passage of a satellite as suggested by Shaya & Tully (2013), or by a concentration of mass in a plane of satellites.

The so called "galactic fountain" model of gas accretion (e.g., Shapiro & Field 1976; Bregman 1980) states that supernovae kick material above the disk of a spiral galaxy, which then rains back down onto the disk as it cools. More recent work has shown that this fountain material can cause the surrounding halo material to condense and fall onto the disk as well (Fraternali & Binney 2008; Fraternali et al. 2015). While the M31–M33 clouds are too far away from either galaxy to be triggered by a galactic fountain, it is possible that hot gas could be triggered to condense by other external sources, such as the motion of a satellite galaxy through the CGM. Such a satellite galaxy would presumably need to contain at least some cold gas to serve as a trigger. It would be interesting to evaluate this mechanism in the context of the M31 CGM.

7. SUMMARY

Prompted by the discovery of extended regions of very faint H I that appear to form a partial bridge connecting M31 and M33 (Braun & Thilker 2004), we have measured 21 cm H I emission in a 12 square-degree region between M31 and M33 with the GBT at 9′.1 angular resolution reaching 5σ limits on $N_{\rm H\,I}$ of 3.9×10^{17} cm^{-2} for a 30 km s^{-1} line. Sensitive observations were also made at 18 locations on a grid to the north of M31.

The new data confirm and extend the basic picture derived from the preliminary data presented in Paper I: in this region between M31 and M33 the H I is largely if not entirely contained in discrete neutral clouds that each have $M_{\rm H\,I}$ reaching a few $10^5 M_\odot$, lying at a projected distance ≈ 100 kpc from M31. We do not find any evidence for a more diffuse component of H I, and attribute our claim for this in Paper I to systematic instrumental baseline effects at the level of a few mK. We measure only 63% of the H I mass found by BT04 in this region. While we present a possible explanation for this discrepancy (Section 3.2), its origin is uncertain. The clouds appear to be spatially and kinematically independent from each other and can have velocities that differ by >100 km s^{-1} over projected distances ~ 10 kpc. Our H I mass limits of $\sim 10^4 M_\odot$ are lower, by an order of magnitude or more, than other surveys of galaxy groups (e.g., Auld et al. 2006; Chynoweth et al. 2008). Thus these objects may represent a new, previously undetected population.

The clouds have a dynamical mass nearly a thousand times their H I mass and strong limits on any stellar component, making it unlikely that they are part of the dwarf galaxy system of the Local Group. Indeed, dwarf galaxies near large spirals in the Local Group completely lack detectable H I (Grcevich & Putman 2009; Spekkens et al. 2014; R. Beaton 2015, private communication; Westmeier et al. 2015). The clouds have kinematics more similar to the systematic velocity of the galaxies than to the HVC system of M31 and M33, but the

clouds have H I properties like those of the M31 HVCs and the class of ultra-compact HVCs (Westmeier et al. 2005, 2008; Adams et al. 2013).

Numerical simulations of the evolution of the Local Group produce regions of neutral gas between the major galaxies that may be analogs to the detected clouds (Nuza et al. 2014), though considerably larger and more massive. If M31 has the very extensive CGM recently proposed by Lehner et al. (2015), then it contains ~ 10 times the column density of gas needed for formation of the clouds at their projected radius. The clouds might then be condensations in the 90% ionized M31 CGM, marking a past interaction with one or more of the dwarf galaxies (Shaya & Tully 2013). It will be critical in understanding the clouds to have an accurate census of the CGM of M31 to determine if the M31–M33 direction is indeed a region of enhanced total mass.

Our results to the northwest of M31 are still too incomplete to determine if we have detected anything like the population of clouds that exists between M31 and M33, but the data do suggest that the HVC population of M31 extends to $\rho \approx 100$ kpc in the northwest, much further than previously known. A similar extension to the southeast is not observed. The detection of H I outside the BT04 contours at $\delta = +47°$ would imply that we are seeing very small angular-sized features that are beam-diluted in the BT04 measurements. Complete mapping of this area with the GBT is underway to resolve the discrepancy.

REFERENCES

Adams, E. A. K., Giovanelli, R., & Haynes, M. P. 2013, ApJ, 768, 77
Auld, R., Minchin, R. F., Davies, J. I., et al. 2006, MNRAS, 371, 1617
Bekki, K. 2008, MNRAS, 390, L24
Bernstein-Cooper, E. Z., Cannon, J. M., Elson, E. C., et al. 2014, AJ, 148, 35
Besla, G., Kallivayalil, N., Hernquist, L., et al. 2010, ApJL, 721, L97
Binney, J., & Tremaine, S. 2008, Galactic Dynamics (2nd ed.; Princeton, NJ: Princeton Univ. Press)
Blitz, L., Spergel, D. N., Teuben, P. J., Hartmann, D., & Burton, W. B. 1999, ApJ, 514, 818
Bono, G., Caputo, F., Marconi, M., & Musella, I. 2010, ApJ, 715, 277
Boothroyd, A. I., Blagrave, K., Lockman, F. J., et al. 2011, A&A, 536, A81
Braun, R., & Burton, W. B. 1999, A&A, 341, 437
Braun, R., & Thilker, D. A. 2004, A&A, 417, 421
Braun, R., Thilker, D. A., Walterbos, R. A. M., & Corbelli, E. 2009, ApJ, 695, 937
Bregman, J. N. 1980, ApJ, 236, 577
Cen, R. 2013, ApJ, 770, 139
Chen, H.-W., Helsby, J. E., Gauthier, J.-R., et al. 2010, ApJ, 714, 1521
Chynoweth, K. M., Langston, G. I., Yun, M. S., et al. 2008, AJ, 135, 1983
Collins, M. L. M., Chapman, S. C., Irwin, M. J., et al. 2010, MNRAS, 407, 2411
Conn, A. R., Ibata, R. A., Lewis, G. F., et al. 2012, ApJ, 758, 11
Conn, A. R., Lewis, G. F., Ibata, R. A., et al. 2013, ApJ, 766, 120
Davé, R., Cen, R., Ostriker, J. P., et al. 2001, ApJ, 552, 473
Davies, R. D. 1975, MNRAS, 170, 45P
de Heij, V., Braun, R., & Burton, W. B. 2002, A&A, 392, 417
de Jong, J. T. A., Harris, J., Coleman, M. G., et al. 2008, ApJ, 680, 1112
D'Onghia, E., & Fox, A. J. 2015, arXiv:1511.05853
Faerman, Y., Sternberg, A., & McKee, C. F. 2013, ApJ, 777, 119
Fox, A. J., Wakker, B. P., Barger, K. A., et al. 2014, ApJ, 787, 147
Fraternali, F., & Binney, J. J. 2008, MNRAS, 386, 935

Fraternali, F., Marasco, A., Armillotta, L., & Marinacci, F. 2015, MNRAS, 447, L70
Fraternali, F., van Moorsel, G., Sancisi, R., & Oosterloo, T. 2002, AJ, 123, 3124
Fukugita, M., & Peebles, P. J. E. 2006, ApJ, 639, 590
Gatto, A., Fraternali, F., Read, J. I., et al. 2013, MNRAS, 433, 2749
Giovanelli, R., Haynes, M. P., Adams, E. A. K., et al. 2013, AJ, 146, 15
Grcevich, J., & Putman, M. E. 2009, ApJ, 696, 385
Grossi, M., Giovanardi, C., Corbelli, E., et al. 2008, A&A, 487, 161
Heald, G., Józsa, G., Serra, P., et al. 2011, A&A, 526, A118
Ibata, R. A., Lewis, G. F., Conn, A. R., et al. 2013, Natur, 493, 62
Kalberla, P. M. W., & Haud, U. 2006, A&A, 455, 481
Karachentsev, I. D., & Makarov, D. A. 1996, AJ, 111, 794
Koch, A., Danforth, C. W., Rich, R. M., Ibata, R., & Keeney, B. A. 2015, arXiv:1506.00635
Lehner, N., Howk, J. C., Thom, C., et al. 2012, MNRAS, 424, 2896
Lehner, N., Howk, J. C., & Wakker, B. P. 2015, ApJ, 804, 79
Lewis, G. F., Braun, R., McConnachie, A. W., et al. 2013, ApJ, 763, 4
Lockman, F. J., Free, N. L., & Shields, J. C. 2012, AJ, 144, 52
Mangum, J. G., Emerson, D. T., & Greisen, E. W. 2007, A&A, 474, 679
Marganian, P., Garwood, R. W., Braatz, J. A., Radziwill, N. M., & Maddalena, R. J. 2006, in ASP Conf. Ser. 351, Astronomical Data Analysis Software and Systems XV, ed. C. Gabriel et al. (San Francisco, CA: ASP), 512
Martin, N. F., Ibata, R. A., McConnachie, A. W., et al. 2013, ApJ, 776, 80
Mayer, L., Mastropietro, C., Wadsley, J., Stadel, J., & Moore, B. 2006, MNRAS, 369, 1021
McConnachie, A. W. 2012, AJ, 144, 4
McConnachie, A. W., Irwin, M. J., Ibata, R. A., et al. 2009, Natur, 461, 66
McQuinn, K. B. W., Skillman, E. D., Berg, D., et al. 2013, AJ, 146, 145
Nichols, M., Mirabal, N., Agertz, O., Lockman, F. J., & Bland-Hawthorn, J. 2014, MNRAS, 442, 2883
Nickerson, S., Stinson, G., Couchman, H. M. P., Bailin, J., & Wadsley, J. 2011, MNRAS, 415, 257
Nidever, D. L., Majewski, S. R., & Burton, W. B. 2008, ApJ, 679, 432
Nidever, D. L., Majewski, S. R., Butler Burton, W., & Nigra, L. 2010, ApJ, 723, 1618
Nuza, S. E., Parisi, F., Scannapieco, C., et al. 2014, MNRAS, 441, 2593
Oort, J. H. 1966, BAN, 18, 421
Oosterloo, T., Fraternali, F., & Sancisi, R. 2007, AJ, 134, 1019
Pisano, D. J., Barnes, D. G., Gibson, B. K., et al. 2007, ApJ, 662, 959
Popping, A., & Braun, R. 2008, A&A, 479, 903
Prestage, R. M., Constantikes, K. T., Hunter, T. R., et al. 2009, IEEEP, 97, 1382
Putman, M. E., Peek, J. E. G., & Joung, M. R. 2012, ARA&A, 50, 491
Putman, M. E., Peek, J. E. G., Muratov, A., et al. 2009, ApJ, 703, 1486
Rhode, K. L., Salzer, J. J., Haurberg, N. C., et al. 2013, AJ, 145, 149
Riess, A. G., Fliri, J., & Valls-Gabaud, D. 2012, ApJ, 745, 156
Ryan-Weber, E. V., Begum, A., Oosterloo, T., et al. 2008, MNRAS, 384, 535
Scannapieco, C., Creasey, P., Nuza, S. E., et al. 2015, A&A, 577, A3
Sembach, K. R., Wakker, B. P., Savage, B. D., et al. 2003, ApJS, 146, 165
Shapiro, P. R., & Field, G. B. 1976, ApJ, 205, 762
Shaya, E. J., & Tully, R. B. 2013, MNRAS, 436, 2096
Shull, J. M., Jones, J. R., Danforth, C. W., & Collins, J. A. 2009, ApJ, 699, 754
Simon, J. D., & Geha, M. 2007, ApJ, 670, 313
Spekkens, K., Urbancic, N., Mason, B. S., Willman, B., & Aguirre, J. E. 2014, ApJL, 795, L5
Stanimirovic, S., Gallagher, J. S., III, & Nigra, L. 2010, SerAJ, 180, 1
Stanimirović, S., Hoffman, S., Heiles, C., et al. 2008, ApJ, 680, 276
Sternberg, A., McKee, C. F., & Wolfire, M. G. 2002, ApJS, 143, 419
Thilker, D. A., Braun, R., Walterbos, R. A. M., et al. 2004, ApJL, 601, L39
Wakker, B. P. 2001, ApJS, 136, 463
Wakker, B. P., York, D. G., Howk, J. C., et al. 2007, ApJL, 670, L113
Wakker, B. P., York, D. G., Wilhelm, R., et al. 2008, ApJ, 672, 298
Westmeier, T., Brüns, C., & Kerp, J. 2005, A&A, 432, 937
Westmeier, T., Brüns, C., & Kerp, J. 2008, MNRAS, 390, 1691
Westmeier, T., Staveley-Smith, L., Calabretta, M., et al. 2015, MNRAS, 453, 338
Wolfe, S. A., Pisano, D. J., Lockman, F. J., McGaugh, S. S., & Shaya, E. J. 2013, Natur, 497, 224
Yun, M. S., Ho, P. T. P., & Lo, K. Y. 1994, Natur, 372, 530
Zwaan, M. A. 2001, MNRAS, 325, 1142